Optimising spherical refraction using a ray-tracing model

An I.C. Student: Sara Capdevila Solé

***Abstract*—A ray-tracing model, made up of variable refracting surfaces was developed and tested. The model allows rays to propagate through lenses of specified curvature, to determine the focal point of convergence of these, and the corresponding RMS spot radius. The algorithm was optimised, by allowing the curvatures to be parameters in the process. This was done by using a Scipy integrated, Nelder-Mead algorithm (fmin). The optimum lens found, was a plano-convex lens with a curvature of the surface facing the rays of $c = 9.50 \times 10^{-3} mm^{-1}$, with a corresponding radial RMS spot size of $RMS = 6.76 \times 10^{-4} mm$, at the circle of least confusion.**

I. Introduction

Lens gather and focus rays of light. These rays can be modelled using ray-tracing methods. In this project, we took into account a non-idealised optical system, where the rays intersected the paraxial plane, around a focal point. This region can be investigated to study the type of aberrations present in the optical system, by calculating the RMS spot size at the focus [1] [2].

The optical system can be optimised, to reduce the degree of the aberrations, as a result increasing the final quality of the image produced.

This report includes additional theory to the project's script [2] on which my model was based, assumptions and testing methods, and a summary of the results and plots obtained.

II. Theory

A. Snell's law

Snell's law is very useful in analysing the behaviours of rays travelling from one medium, into another, with refractive indexes, n_1 and n_2 correspondingly. This is visible in fig. 1.

A vector form representation of the law is the following;

$$n_1(\mathbf{i} \times \mathbf{n}) = n_2(\mathbf{t} \times \mathbf{n}), \tag{1}$$

where $\mathbf{i}$ and $\mathbf{t}$ are the unit incident and transmitted vectors respectively, and $\mathbf{n}$ is the unit normal to the surface between the two mediums.

Using (1), an expression for the transmitted vector can be found [3]. This can be used to propagate the rays across the surface.

B. Lens makers equation

To calculate the theoretical, focal point of the lens, the lens maker's formula [4] was used. The equation takes into account the curvatures of the two surfaces of the lens, c_1 and c_2, and their centre, Z_c;

$$f = Z_c + ((\frac{n_2}{n_1} - 1)(c_1 - c_2))^{-1}. \tag{2}$$

This was used in the testing (section III) of the model.

C. Bundle

A mathematical model was created to mimic a beam of light. This model generated collimated rays of uniform intensity, by diving the beam into 6 invisible concentric rings. For the density of the rays to be the same at any point within the cross-section of the beam, each ring had to have equally spaced out rays. The class allows for the diameter of the beam to be an input, although its default value was set to 10mm. An example of a bundle of rays interacting with a spherical surface can be seen in fig. 3.

D. RMS spot radius at focus

The method generating rays as a bundle, propagated them along the $Z-axis$. To locate the circle of least confusion of the converging rays, the minimum radial spot size was calculated, using the average root mean square method (RMS), taking the corresponding x and y positions of the each ray at the specified output plane ($Z-$coordinate), using the following equation [1];

$$RMS = \sqrt{\frac{\sum_{i=1}^{N} x_i^2 + y_i^2}{N}}, \tag{3}$$

where N is the total number of rays in the bundle. The corresponding $Z-$value minimising the RMS was then used to find a more accurate location for the focal point of the specific lens.

III. Testing

As a result of the non-idealised optical model, the rays will only behave as described in (2), whenever Fermat's lens requirements are met [4]. This model will deviate from the ideal behaviour as the distance of the generated rays from the paraxial plane is increased, and the lens thickness and aperture increases, creating spherical aberrations. This is due to (2) being derived from a parabolic shaped lens (the surfaces are more curved in reality as the distance from the optical axis increases).

A lens surface was implemented into all plots, to verify refraction took place at the points of specified curvature. Additionally, (2) was used to calculate the focal range, checking its compatibility with my model. Simple-test cases, on spherical surfaces, were tested in task 11 for appropriate convergence and focal point location. These are shown in fig. 2.

Every task, before being implemented into the model, was tested individually in small subsections. This was done to improve the accuracy and time efficiency of the code (e.g. Execution times was compared using Pythons $timeit$ module).

Debugging and inconsistencies were easier to overcome as a result.

IV. Lens optimisation

Specific formulae were devised to calculate the minimum RMS spot radius as an optimisation metric for a specified curvature, for each lens, biconvex and plano-convex. Using a Scipy integrated optimise function, fmin, based on the Nelder–Mead method, optimisation was solely based on function values (not derivatives), to find the optimum curvatures that produced the best-form lens, with a locally minimised RMS spot radius. This function requires an initial guess of the minimum, which was of the order of $10^{-2}mm^{-1}$.

The following parameters were used for finding the optimised lenses. The centre of the first surface, $Z_0 = 100mm$, with a separation between the surfaces of $10mm$. The aperture radius of the lens, $r_a = 5mm$.

A. Results

The singlet biconvex lens, taking both curvatures as parameters for optimisation, had an minimised RMS spot radius of $RMS = 4.69 \times 10^{-3}mm$, at a focus of $f = 198mm$, with lens curvatures of $c_1 = -c_2 = 1.08 \times 10^{-2}mm^{-1}$.

The plano-convex lens, with the curved surface facing the rays; $RMS = 6.76 \times 10^{-4}mm$, $f = 307mm$, with $c = 9.50 \times 10^{-3}mm^{-1}$. This same lens, with opposite orientation, had an optimised RMS spot radius of $RMS = 2.86 \times 10^{-3}mm$, at a focus of, $f = 308mm$, with $c = -9.75 \times 10^{-3}mm^{-1}$.

A visualisation of the performance of each lens can be seen in figs. 4, 5.

The rays interfering with the symmetrical biconvex lens, converge at a focus much closer in comparison to the other lenses. This agrees with their expected behaviour, as they are known to optimise close-lens imagining [4]. This would be interesting to investigate further.

As expected, for rays coming parallel to the $Z-$axis, the best-form lens was the plano-convex lens, with the curved surface first [5]. In all cases, due to the non-idealised nature of the model, the source of the aberrations were the peripheral rays being more strongly focused than the paraxial rays, intercepting the $Z-$axis before the focal point. This is due to peripheral rays, having a larger ratio of their distance from the optical axis, to the radius of curvature of the lens. The spherical shape of the lens becomes more apparent and thus diverges from the parabolic approximation (ie. the 'ignored' terms in the derivation of (2) become more significant). This can be clearly seen in fig. 6.

As a means of visualising the optimisation process, and as a form of proof that the optimum curvatures found minimised the RMS spot radius, a plot for the plano-convex lens, comparing both orientations was produced, shown in fig. 7. Both curves present a comparable resemblance, but surprisingly, at some specific curvatures, the optimised RMS is smaller for the plano-convex lens with the plane surface facing the rays, however, the form with the convex surface first, still has a lower average RMS throughout, significantly remarked at its optimum curvature.

For a 3-Dimensional visualisation, fig. 8. shows the complete performance of the optimised best-form plano-convex lens, to an output plane at $Z = 500mm$.

V. Limitations and ideas for improvement

As previously outlined, most limitations to the model, originated for larger off-axis rays, due to the spherical curvature of the lens. I also had to take into account the separation between the surfaces, to limit ray deviations within the lens, however, this wasn't always ideal, as the surfaces shouldn't overlap in regions where ray propagation took place. For example, for the optimised lenses, the calculated focus (f_c) diverged slightly from what was modelled; the plano-convex lens, with the convex surface facing the rays; $f_c = 310mm$, for the plane surface facing the rays; $f_c = 315mm$, for the biconvex lens, however, the focal point was the same. As a result, to locate the circle of least confusion, my model seems to hold to 2 significant figures.

If I was to continue working on this model, I would focus on finding different ways of optimising the curvatures of lenses, and also on representing this optimisation process in plots, as looping through the function was very time inefficient. An approach could be to use the alternative methods, such as those $Scipy.optimize.minimize$ provides, making a $deepcopy$ of the path of the results. This would involve using various other methods of numerical minimisation, including Powell's, BFGS and the Newton-Raphson method, to name a few. This would provide more tools to investigate the optimisation process for the biconvex lens, with two variable curvatures.

Another characteristic of the model I would like to address would be the circle of least confusion, resulting in spherical aberrations. It'd be interesting to design an optical system to correct this, with a multi-lens system approach, similar to that of a camera lens (e.g. smartphones) [5]. Otherwise, implementing the functioning of the human eye, as a system of gradient-indexed lenses, which have a varying refractive index in the radial direction, could also be tested to eliminate spherical aberrations [6].

References

[1] Hesam Mahmoudi Nezhad, Neda. (2014). Optical System Optimization Using Genetic Algorithms. 10.13140/RG.2.2.18066.68803.

[2] David Colling, Carl Paterson and Robert Kingham. (2020). Imperial College Physics Y2 Computing - Short Projects (v2.3.1). Project A: An Optical Ray Tracer.

[3] Antonín Mikš and Pavel Novák. (2012). Determination of unit normal vectors of aspherical surfaces given unit directional vectors of incoming and outgoing rays: Optical Society of America, page 1356.

[4] Mike Damzen. (2019). Imperial College Physics Y1 - Optics Course - 4. Imaging with Spherical Lenses Mirrors.

[5] $Thorlabs$. (2020). Lens tutorial. Accessed: (04/11/20). Link: [https://www.thorlabs.com/tutorials.cfm?tabID=BA49B425-F85B-4549-8C1A-F111DDBB9099]

[6] Hecht, Eugene; Zajac, Alfred (1987). Optics (2nd ed.). Reading, Mass.: Addison-Wesley. p. 178. ISBN 978-0201116090. OCLC 13761389

VI. Plots

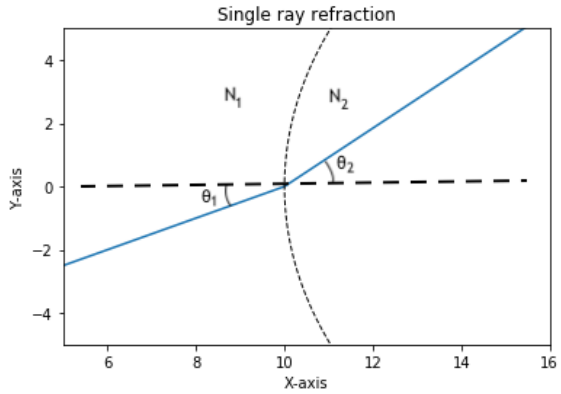

Fig. 1. Visualisation of Snell's law function using one ray.

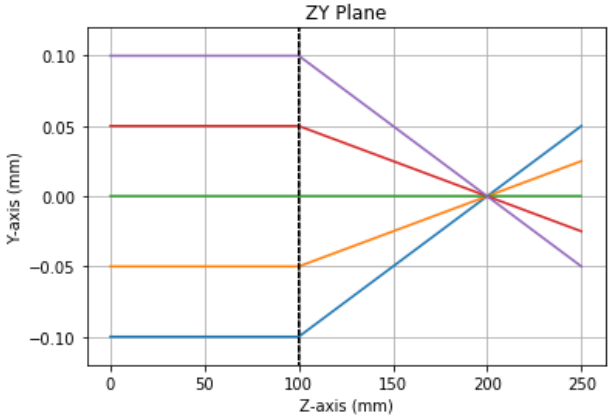

Fig. 2.1. Test case of lens with rays coming from air into glass, $c = 0.03\ mm^{-1}$.

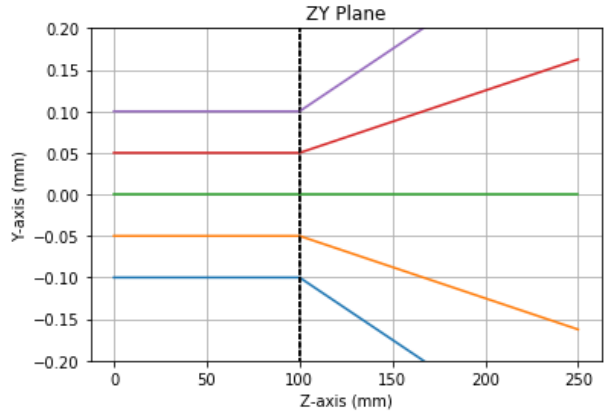

Fig. 2.2. Test case of lens with rays coming from glass into air, $c = 0.03\ mm^{-1}$.

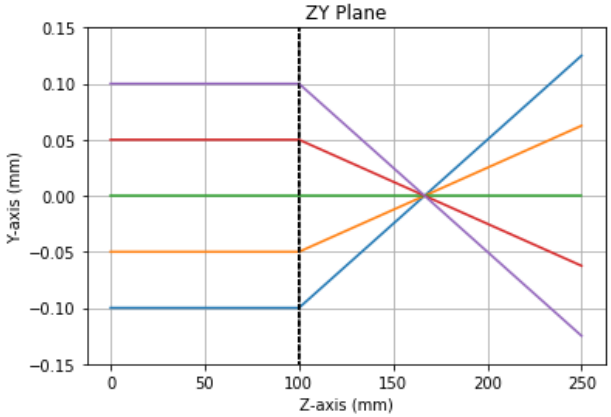

Fig. 2.3. Test case of lens with rays coming from glass into air, $c = -0.03\ mm^{-1}$.

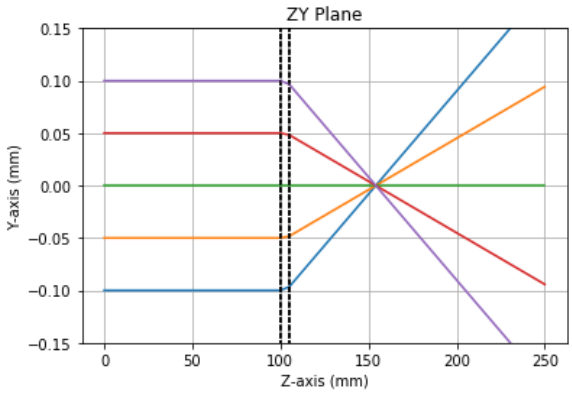

Fig. 2. 3. Test case of lens with two surfaces, $c_1 = 0.02\ mm^{-1}$ and $c_2 = 0.02\ mm^{-1}$, approximately $f = 150\ mm$.

Fig.2. Plots for additional simple test-cases.

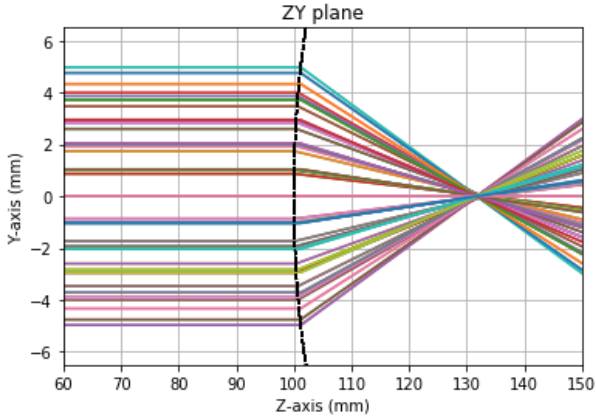

Fig. 3. Tracing a large-diameter uniform bundle of collimated rays through a spherical surface, $c = 0.09\ mm^{-1}$.

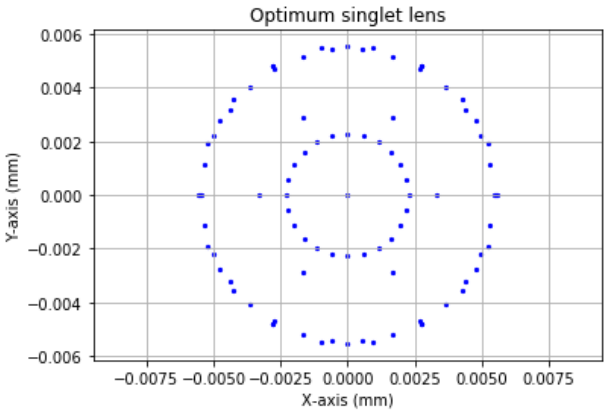

Fig. 4. 1. Biconvex lens.

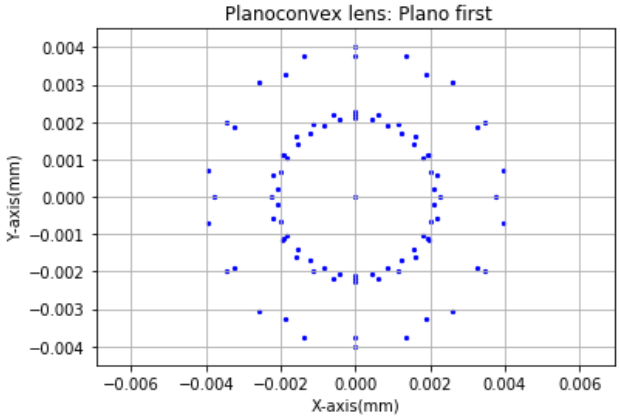

Fig. 4. 2. Plano-convex lens with convex surface facing rays.

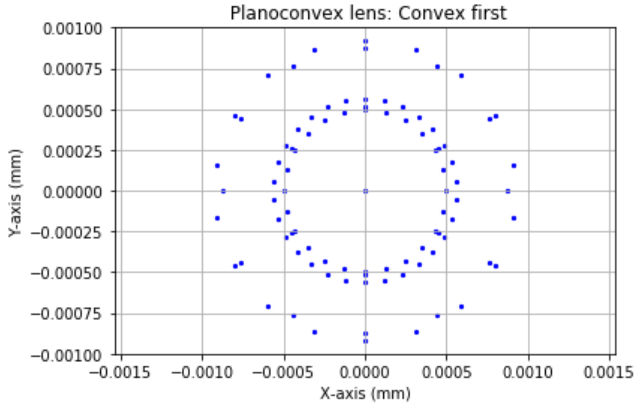

Fig. 4.3. Plano-convex lens with plane surface facing rays.

Fig. 4. Spot diagram for the bundle of rays, at the paraxial focal plane, for each corresponding lens at its optimum curvatures.

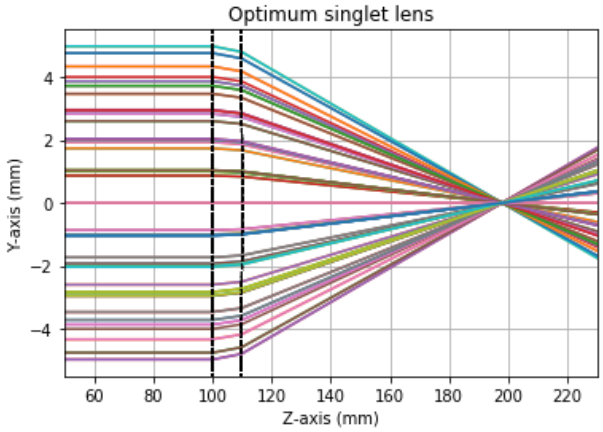

Fig. 5. 1. Biconvex lens.

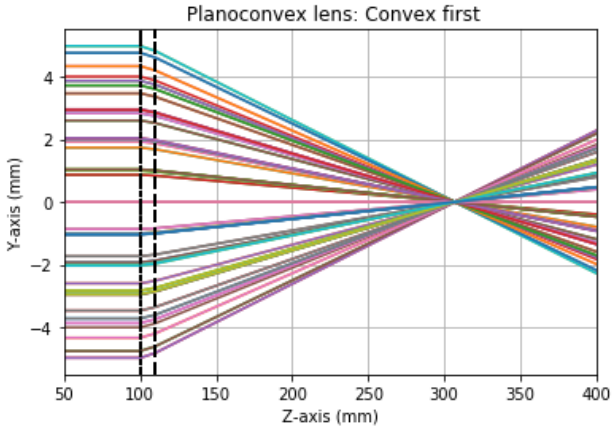

Fig. 5. 2. Plano-convex lens with convex surface facing rays.

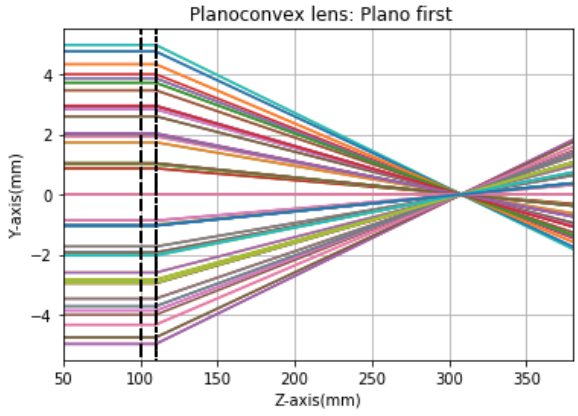

Fig. 5. 3. Plano-convex lens with plane surface facing rays.

Fig. 5. Ray trajectories in the ZY-plane for the optimised corresponding lenses.

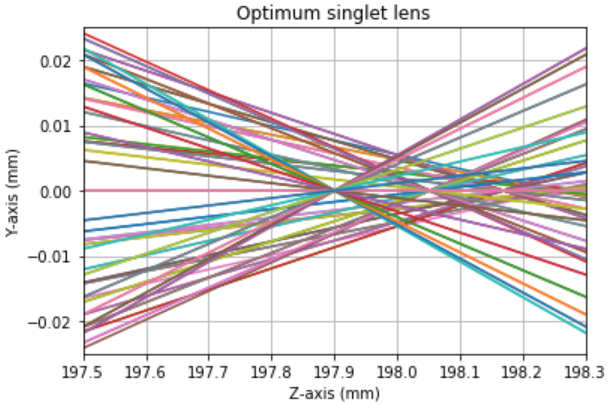

Fig. 6. 1. Biconvex lens.

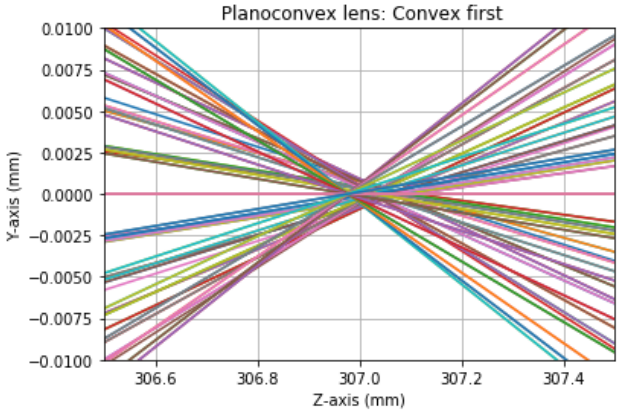

Fig. 6. 2. Plano-convex lens with convex surface facing rays.

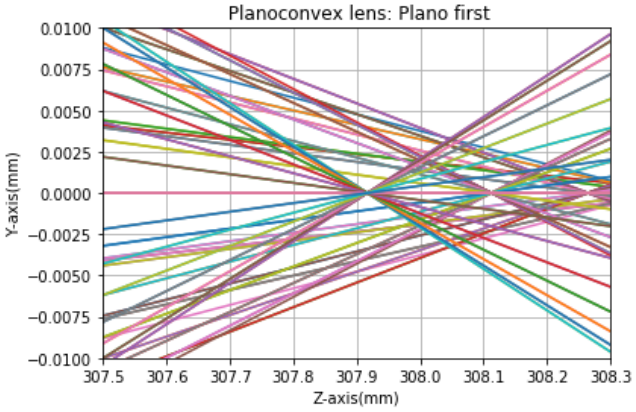

Fig. 6. 3. Plano-convex lens with plane surface facing rays.

Fig. 6. 2D performance representation - circle of least confusion for each corresponding optimised lens.

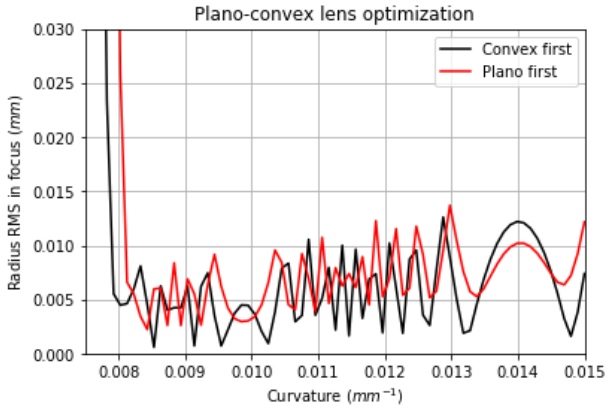

Fig. 7. Optimisation curves showing how the optimised radial RMS varies with magnitude of the curvature in both orientations of plano-convex lenses.

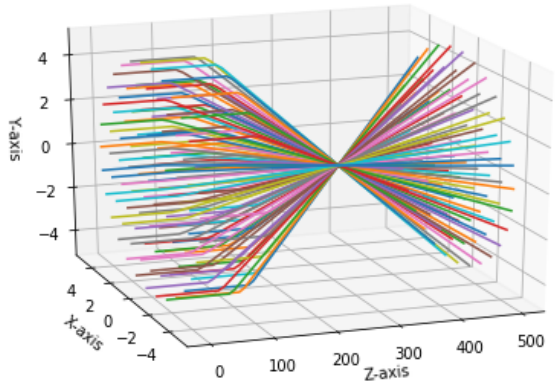

Fig. 8. 3D representation of rays passing through the optimised plano-convex lens, with the convex surface facing the rays.